




Fabrication of low cost nano-grass n-type C-Si solar cell with sol–gel Al_2O_3 passivation

Soma Ray^{1,2} · Anup Mondal³ · Utpal Gangopadhyay¹ Received: 6 May 2020 / Accepted: 30 September 2020 / Published online: 26 October 2020
© Springer Nature Switzerland AG 2020

Abstract

Silicon nano-grass Solar cell has the advantage of enhancing efficiency with cost effective method. Highly ordered silicon nano-grass is formed by chemical etching process. During this chemical etching unwanted nanograss is formed on both side of the wafer, resulting considerable transmission loss from rear side. This results in ultimate reduction of efficiency. The detrimental effect of nano-grass formation on both side of the wafer is briefly demonstrated here by simulation methods. Adopting the idea by simulation method this paper has reported silicon front sided nano-grass n-type c-Si solar cell by spin on diffusion source and rapid thermal annealing. The sheet resistance of the nano-grass silicon wafer is varied with respect to different spin-on diffusion profile. Later front surface has been passivated by sol–gel Al_2O_3 passivation. Eventually all the spin doped silicon nano-grass solar cell with sol–gel Al_2O_3 passivation provides a very promising route of cost effective high efficiency silicon solar cell technology. Broadband reflection between 300 and 1100 nm wavelengths has been suppressed to 2% for nano-grass Solar cell and maximum efficiency of 16.57% is achieved.

Keywords Texturization · Nano-grass · Passivation · Sol–gel · Short circuit current

1 Introduction

Present Solar cell technology is highlighted on low cost and easy fabrication process [1]. In this aspect electrical and optical properties of Solar cell have been introduced by some cost effective technique. There are different types of antireflection coating in the commercial production scale to reduce the reflectance [2, 3]. Although the coating shows good optical property but the budget is high due to sophisticated fabrication unit. To reduce to reflectance more with low cost process silicon nanowire structure is introduced [4]. The structure has been formed by several fabrication methods like chemical vapor deposition (CVD) reactive ion etching (RIE), vapor Liquid Solid (VLS), metal assisted chemical etching (MACE) [5]. Metal assisted chemical etching is most suitable technique which not only

improves the optical property but also reduces production cost considerable [6]. In metal assisted chemical etching process most vital chemical is HF (hydrofluoric acid). HF helps to etch the silicon by forming H_2SiF_6 (hydro-fluoro-silicic acid) [7]. Instead of this the main drawback of silicon nanowire structure by HF is that the reaction rate is very high in this process for which the process is uncontrolled and reaction chemical aging is poor. Moreover bundle and pore formation occurs in this process very easily due to uncontrolled and high reaction rate [8]. Silicon nano-grass was introduced in this paper to avoid these drawbacks. This structure reduces the reflectance over broadband region and Silicon nano-grass is such a useful technology to enrich the optical property of Solar cell by reducing the reflectance over broadband wavelength region. During this chemical etching nano-grass was formed on both

✉ Utpal Gangopadhyay, utpal_ganguly@yahoo.com | ¹Centre of Advanced Research in Renewable Energy and Sensor Technology, Meghnad Saha Institute of Technology, Nazirabad, Uchhepota, via-Sonarpur, Kolkata 700150, West Bengal, India. ²Centre of Excellence for Green Energy and Sensor Systems, IEST, Shibpur, Howrah 711103, India. ³Department of Chemistry, IEST, Shibpur, Howrah 711103, West Bengal, India.



side of the wafer resulting enhancement of transmission followed by absorption loss so front surface nano-grass structure was preferable one. In this paper comparison of solar cell performances for single side and both side of the nanowire were shown. Optical property was analysed by opti-FDTD software and the electrical property analysis was done by SILVACO TCAD software by merging the optical data. Performance of the proposed device was analysed with respect to the influence of nanoglass on one side and both sides on short circuit current, open circuit voltage, fill factor and efficiency. Due to lower transmission loss of front sided nanoglass Solar cell, efficiency was higher than both sided nanoglass Solar cell. To make single sided nanoglass here we have prepared an acid resistance polymer TP-2019 (in-house developed polymer) to protect the rear side of the silicon. Silicon nanoglass was grown only in front surface by coating the polymer on rear side. SOD (spin on doping) and RTA (rapid thermal annealing) were particularly necessary for shallow junction diffusion. High temperature annealing with rapid temperature rise and drop reduced thermal budget [9]. In this paper we have used SOD and RTA for diffusion over silicon nano-grass structure. Different temperature RTA diffusion profile was taken here in which the temperature and also the process time were varied. The sheet resistance was monitored for different RTA profile. In commercial purpose ALD was used as passivation unit which increased the processing cost [10]. In this paper passivation the process was done by sol-gel method to reduce the cost. Surface morphology has been studied in this paper. Passivation effect was determined by lifetime enhancement. Complete solar cell characterization has been studied and the finished ultimate solar cell gave above 16% efficiency. Schematic

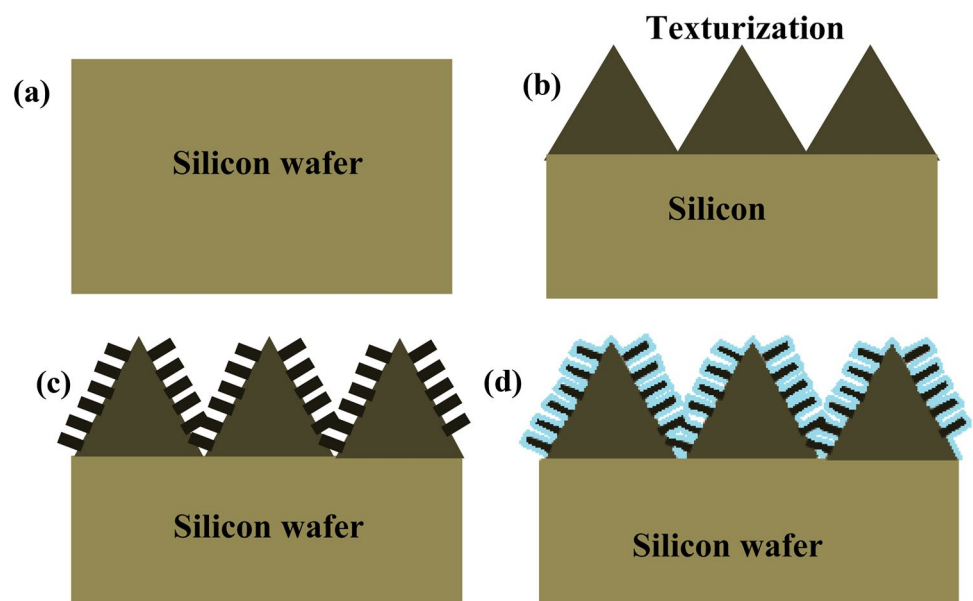
diagram of silicon nano-grass textured silicon with Al_2O_3 coating was shown in Fig. 1

2 Experimental method

N-type c-Si with area 58.6 cm^2 and resistivity $2\text{--}5 \ \Omega\text{cm}/\square$ was taken for experimental purpose. The surface of the wafer was texturized by 2% KOH/6.5%IPA/NaOCL solution at $82 \text{ }^\circ\text{C}$ for 4 min. The surface was cleaned by HF aqueous solution. To form only front surface nano-grass, rear surface of the wafer first covered by an acid resistance polymer TP-2019 (in-house developed polymer). Silicon nano-grass structure was formed by $\text{NH}_4\text{F}/\text{H}_2\text{O}_2/\text{AgNO}_3$ solution for 3 min. The structure was formed by two step etching process. In the first step Ag nanoparticles was embedded on silicon by immersing in $\text{AgNO}_3/\text{NH}_4\text{F}/\text{H}_2\text{SO}_4$ solution for 30 s and next the oxide layer formed by H_2O_2 was removed by forming H_2SiF_6 followed by dipping the wafer for 3 min in $\text{H}_2\text{O}_2/\text{NH}_4\text{F}/\text{H}_2\text{SO}_4$ solution.

For boron diffusion on emitter surface we used spin on dopant source B155 (Filmtronics). The source material was kept at room temperature for at least 20 min to avoid coagulation of the liquid. Spin coating on the surface of the wafer has been done at 3500 rpm for 30 s. Then the SOD samples were heated in baked furnace for $250 \text{ }^\circ\text{C}$ for 15 min. Diffusion was done by rapid thermal annealing process. Profile temperature was varied from 920 to $960 \text{ }^\circ\text{C}$. Whole process was done in nitrogen ambient. Oxidation time varied for different profile. Ramp up and ramp down temperatures were varied successively with sample. The oxide surface formed after thermal annealing was removed by etching in HF aqueous solution. In

Fig. 1 Schematic diagram **a** Silicon wafer **b** textured silicon **c** nano-grass textured silicon **d** of Al_2O_3 coated textured silicon nano-grass structure



the rear side of the sample phosphorous doping was done by same SOD profile with P-509Filmtronics. Process sequence was same as before. Spin coating time and rpm were kept same. Thermal annealing was done at 850°C. Furnace ambient was kept same as of boron diffusion.

Sol-gel passivation by Al_2O_3 was done on silicon by starting from 1.5 M aluminum nitrate $\text{Al}(\text{NO}_3)_3$ dissolved in 2-methoxy ethanol (15 ml). Then this solution was stirred for 40 min. Monoethanolamine 0.602 ml was added to the solution and the solution was constantly agitating by magnetic stirrer at room temperature for 2 h to get a transparent solution. This prepared alumina solution was filtered by PTTE membrane. This was coated on the emitter surface of textured silicon nanograss diffused material.

Front and rear side metallization was done by conventional metallization process followed by baking and firing. Metallization by screen printing on front side was occurred by Ag/Al paste while rear side by Ag paste followed by baking at 300 °C. Firing temperature was kept between 800–850 °C.

3 Device simulation

There are two types of losses generally occurred in Solar cell like electrical loss and optical loss. To simulate Solar cell these two losses were taken into account. For optical analysis nanograssSolar cell structure has been simulated by OPTI-FDTD software. In this analysis we have contemplated silicon nanograss with height 200–300 nm with diameter 50–100 nm, which were equally distributed all over the surface. Our objective was to compare the performance of front sided nanograss with both sided nanowire in silicon solar cell. For nanowires, if the lengths of the nanograss were within the range of nanometer an unusual incident would happen. In this condition light could not recognize the surface texture of c-Si as plane surface and thus no scattering happens [11]. For this reason the measurement of reflection of light through the nanowire surface could not be determined by the Fresnel's theory of ordinary reflection and transmission [12, 13]. Here we must took into account the Maxwell's electromagnetic theory for calculating reflection and transmission for TE and TM wave [13]. To calculate reflectivity, effective medium theory has to be considered [11]. Effective medium theory was applicable for the medium where we subdivide the medium in smallest constituents and averaging all to find more precise result [13, 14]. This could be done by modeling of effective medium theory which describes the effective refractive index of smallest individual parts of a nanowire [11, 15].

When the cell was illuminated with sunlight, carriers will be generated due to photon excitation. From the rate of generation of the carriers G could be calculated as

$$G = \alpha N_0 e^{-\alpha x} \quad (1)$$

where, N_0 was the photon flux density, which was equal to

$$\frac{\text{power}(W/m^2)}{\text{photonflux}} \quad (2)$$

and following Sympson's 1/3 rule, total G can be evaluated [16, 17]. More generation of carriers will lead to higher short circuit or light generated current which was proportionally related to G as J_{sc} or

$$J_L = qG(L_n + L_p) \quad (3)$$

[18, 19]. Another important factor was that with the rise in surface recombination velocity (SRV) J_{sc} is reduced. This happened because of the decrease in diffusion length of electrons (L_n) and holes (L_p) with SRV, which was found from the equations

$$L_n = \sqrt{D_n \tau_{neff}} \quad (4)$$

[17] and

$$L_p = \sqrt{D_p \tau_{peff}} \quad (5)$$

[20].

To perform the electrical analysis the device structure has been simulated by SILVACO TCAD software. The total program has three parts: define structure, diffusion, numerical resolution [20]. We have introduced and merged the reflection and transmission data of opti-FDTD with SILVACO TCAD program. The total program in SILVACO was written in ATLAS mode [21]. After defining the structure diffusion profile was imported. In beam structure we have incorporated the optical data profile from externally. The contact structure was defined by cathode metal. Figure 2 showed OPTI-FDTD simulation for single and double sided nanograss silicon structure.

4 Results and discussions

4.1 Simulation result

In opti-FDTD simulator we have created the structure first. Obtained silicon nanograss on front and both surface of silicon wafer were shown by the diagram found by opti-FDTD. Simulated reflected and transmitted graph were shown in Fig. 3. The wavelength range of interest was taken from 300 to 1100 nm, where absorption

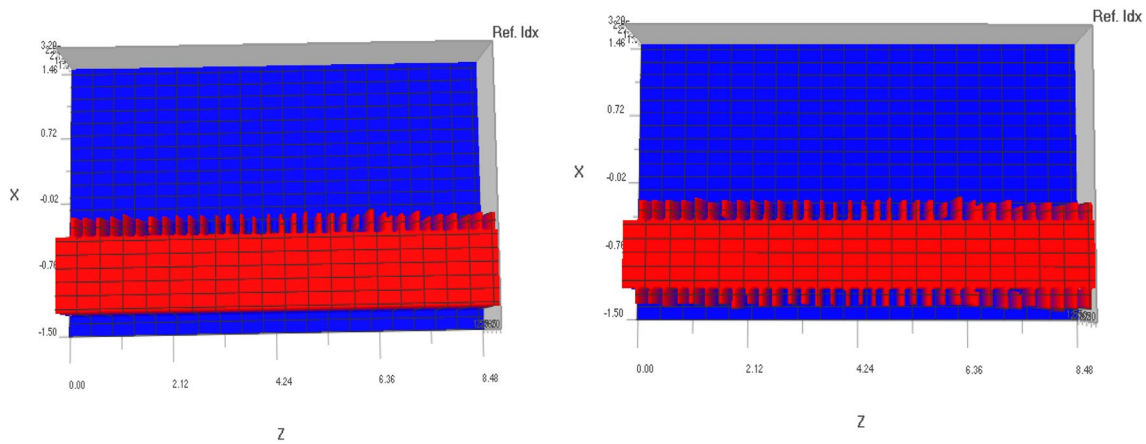
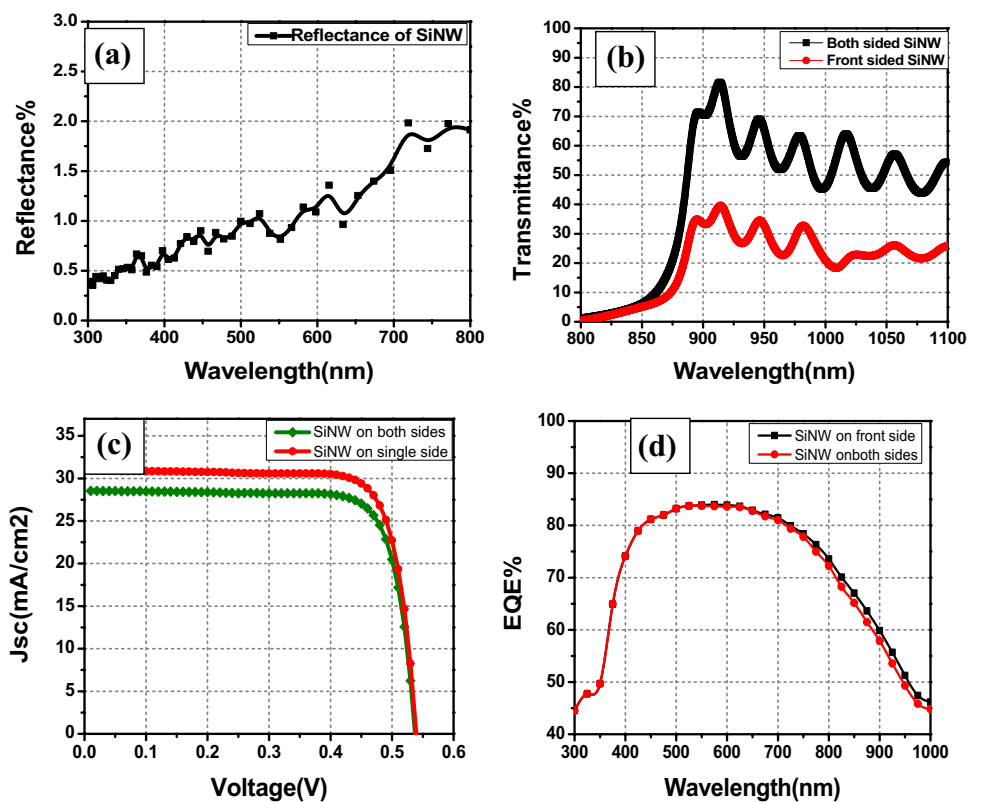


Fig. 2 Simulation structure (by OPTI FDTD) of single and double sided nanograss

Fig. 3 **a** Reflectance analysis **b** Transmission analysis **c** I-V characteristics curve **d** EQE analysis of single and both sided nanowire



coefficient of silicon was highest. After optical simulation by opti-FDTD software reflection and transmission graphs were procured. Reflection graph data revealed an enormous reduction of reflectance over broadband region. Less than 2% reflection was found for UV–VIS spectral region. In transmission graph it was shown that average transmittance increases after formation of both sided nanograss. 40% additional transmission loss has occurred for both sided nanograss for wavelength 920 nm. This loss reduced ultimate conversion efficiency.

Diffusion was taken only front side of the wafer to reduce complicity.

Figure 3c depicted I–V characteristic curve of simulated silicon nanograss Solar cell by SILVACO. Silicon nanograss on both sides of the solar cell showed poor quality J_{sc} than silicon nanograss on single side of the Solar cell. Total Solar cell charecterization data including J_{sc} , V_{oc} , FF and Eff for SiNG for front surface and both surface of the wafer was shown in Table 1. Above 1% efficiency enhancement occurred for single surface nano-grass wafer. We have

Table 1 Solar cell performance theoretically for single sided and both sided nanowire wafers

Wafer type	Jsc (Theo)	Voc (Theo)	FF (Theo)	Eff (Theo)
SiNG on front side	30.89	538.55	0.795	13.21
SiNG on both side	28.53	538.55	0.7982	12.13

Table 2 Variation of sheet resistance (Rsh) for different emitter diffusion profile samples

Sample number	Temperature (°C)	Time (min)	Rsh (ohm/sq.)
#S1	920	25	38–40
#S2	940	18	50–55
#S3	960	4	45–50
#S4	930	13	60–70
#S5	928	15	75–77

simulated the external quantum efficiency (EQE) data. EQE was the number of photons actually entered and which was responsible to create electron hole pair in the Solar cell. This parameter was responsible entirely on optical and electrical parameter of the cell. For both sided nanogras-solar cell more optical loss occurred from rear side of the wafer causing reduction of EQE. This result was also validating the experimental graph. Around 85% peak EQE was found at 550 nm wavelength.

4.2 Sheet resistance measurements

Sheet resistance (Rsh) of different diffusion profile of RTA diffused SOD samples were carried out by four probe unit. Sheet resistance was varied with different diffusion profile and has shown in Table 2. Highest sheet resistance has been observed for #S5 sample. The peak temperature of the batch was 928°C and the stabilization time was 15 min. 75–77 Ω/\square sheet resistance was found for #S5 sample whereas 38–40 Ω/\square for #S1 sample. The temperature and stabilization time was 920°C for 25 min. For highest obtained sheet resistance RTA diffusion profile has shown in Fig. 4a. In this picture the linear ramp of the temperature occurred up to 6 min after which the process time started. O₂ supply was initiated at this stage and the supply was stopped at the end of process time.

Stabilization period at which highest temperature was kept constant and in this case it started after 7 min and ended on 35 min. The total process has been done in N₂ atmosphere. To check the diffusion uniformity sheet resistance has been measured for 1 cm apart and the result is shown in Fig. 4b. Here we have seen #S3 and #S4 samples have non uniform sheet resistance require betterment of

diffusion process. #S5 sample showed good uniformity. Sheet resistances were within 75–77 Ω/\square .

ECV profiles Fig. 4c of samples from #S1 to #S5 has been measured after completing solar cell processes. The depth profile and surface concentration signifies differently doped emitter. With enhancement of sheet resistance junction depth reduces.

In similar manner sheet resistance of rear side diffusion was measured. Variation of Rsh was within 30–35 ohm/sq for all samples (Table 3). It was not varied much as the deposition and process parameter on the rear side diffusion was kept same.

4.3 FESEM and EDAX study

Surface analysis was carried out by FESEM study with different magnifications. Figure 5a showed FESEM study of textured silicon. The height of the pyramid was around 3–4 μm . Silicon nano-grasses were grown on all over the pyramidal surface uniformly. Figure 5b depicted grown of sol–gel Al₂O₃ layer on plain silicon wafer. The layer was cracked due to high thickness. Figure 5c showed Al₂O₃ on textured nano-grass silicon. The surface defined grown of Al₂O₃ on all over the surface of nano-grass textured silicon. The black portions were cracked portion and Fig. 5d showed Al₂O₃ on textured nano-grass wafer with higher magnifications. For textured nano-grass sample thickness of Al₂O₃ was optimized and a typical FESEM result was shown. The valley seemed to have thicker Al₂O₃ coating while the peaks are relatively lower thickness. The surface cracking occurred mainly due to high temperature treatment of annealing. The layer was in homogeneously dispersed on the surface of the nano-grass. Sample roughness enhanced the probability of surface cracking of Al₂O₃ film. The microanalysis of as deposited thin film of Al₂O₃ was shown in Fig. 5e by EDAX analysis. The observed peaks were silicon along with aluminum and oxide.

4.4 Lifetime measurement and Solar cell characterization

Surface analysis of Al₂O₃ passivation layer was examined by measurement of lifetime using semilab lifetime tester. Enhancement of lifetime with annealing temperature ensured the passivation effect. Maximum lifetime obtained at temperature 500 °C (Fig. 6). It has reached up to 210 μs . More modification of sol–gel passivation will make ensure betterment of passivation effect followed by enhancement of surface carrier lifetime.

The finished cells were characterized by solar simulator software. Figure 7 ensured the experimentally obtained data. From this analysis it was cleared that #S5 provides highest efficiency. This was due to betterment of surface

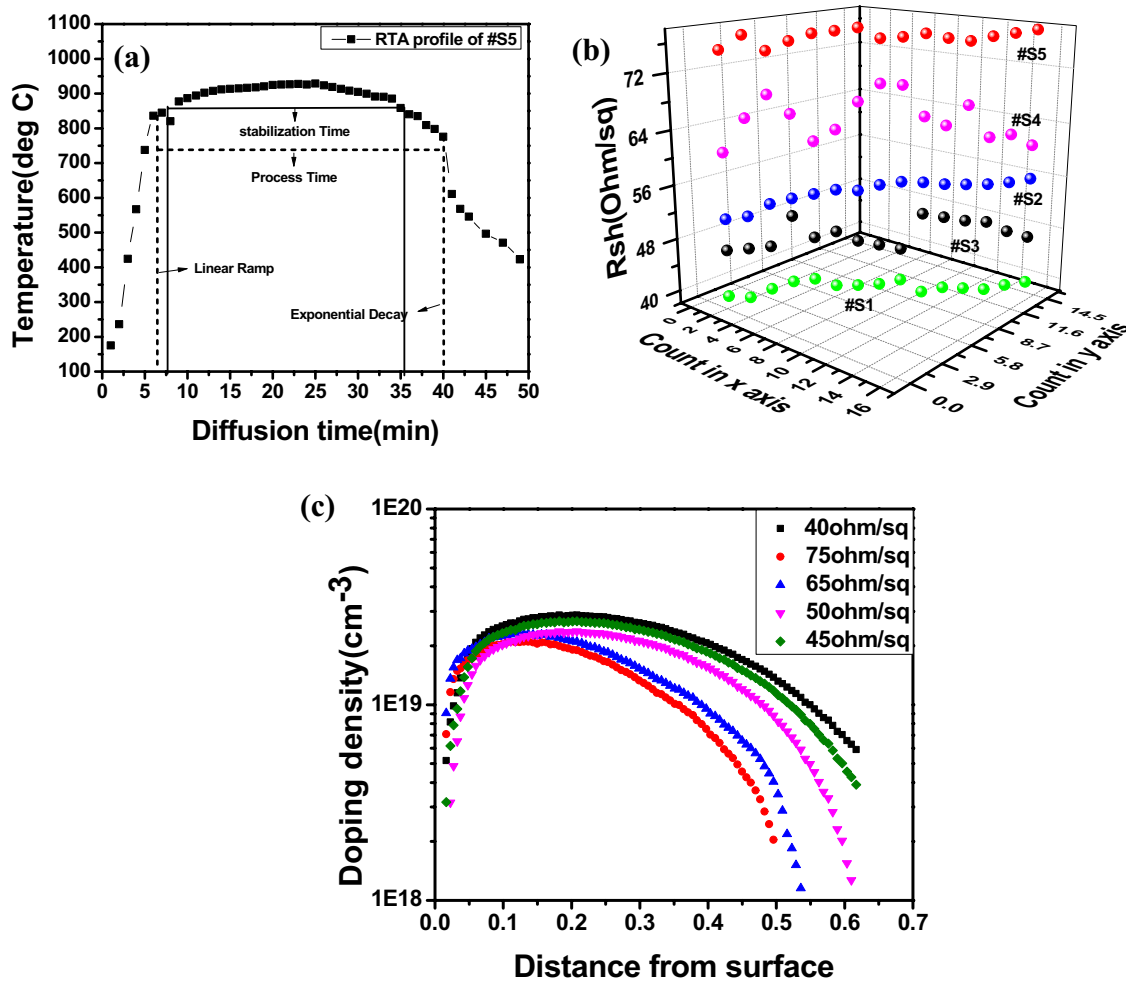


Fig. 4 a Typical RTA diffusion profile of #S5, b variation of R_{sh} in a sample with distance apart, c ECV profile of #S1 to #S5 samples

Table 3 Variation of sheet resistance (Rsh) for different rear diffusion profile samples

Sample number	Temperature (°C)	Time (min)	Rsh (ohm/sq.)
#S1	850	20	30–35
#S2	850	20	32–34
#S3	850	20	32–35
#S4	850	20	30–33
#S5	850	20	30–34

diffusion. Short circuit current density (J_{sc}) and also open circuit voltage (V_{oc}) were higher in this case than other samples. This caused 16.57% efficiency. In #S4 sample efficiency dropped near 1%. #S1 provided lowest efficiency along with open circuit voltage due to lower sheet resistance in diffusion profile as shown in Table 2. Diffusion played a crucial role in solar cell efficiency enhancement.

This step defined the junction depth followed by how much carrier would collect in the junction and total charge collection in the junction enhanced short circuit current and open circuit voltage. Betterment of shunt and series resistance was totally predominated by the diffusion parameter, so fill factor (FF) varied accordingly and also short circuit current and open circuit voltage. Here series resistance would not vary much as nanowire fabrication and metallization of solar cell was kept same in all cases.

5 Conclusion

Present solar cell technology has been largely emphasized on low cost and easy fabrication technique. Silicon nano-grass structure was going to be a trending technology in solar photovoltaic field due to its cost effective and easy fabrication technique. The process was done mainly by chemical etching. During the etching

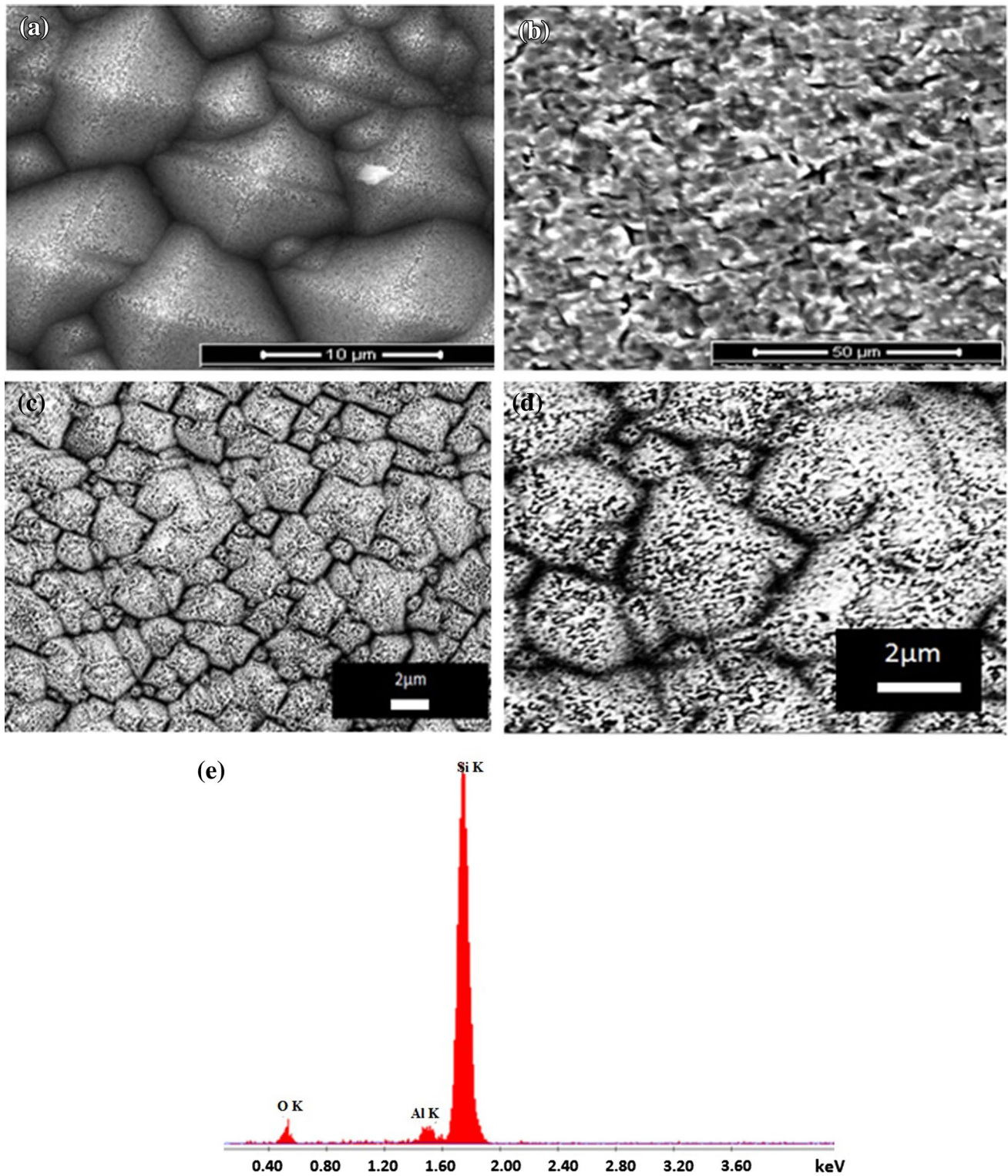


Fig. 5 FESEM of **a** textured nano-grass sample, **b** sol-gel Al₂O₃ coated base silicon wafer, sol-gel Al₂O₃ coated textured nano-grass silicon **c** with magnification 5K \times , **d** with magnification 15K \times , **e** EDAX of Al₂O₃ coated silicon

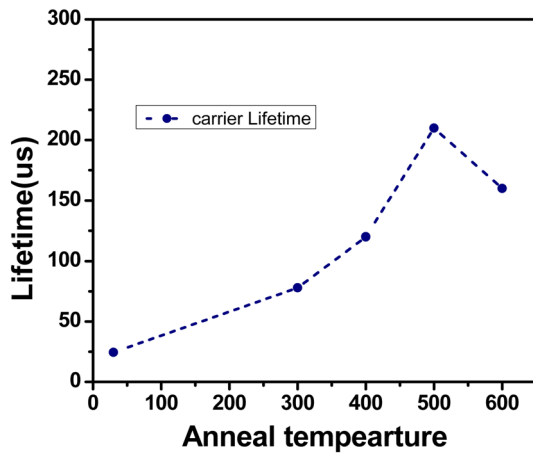
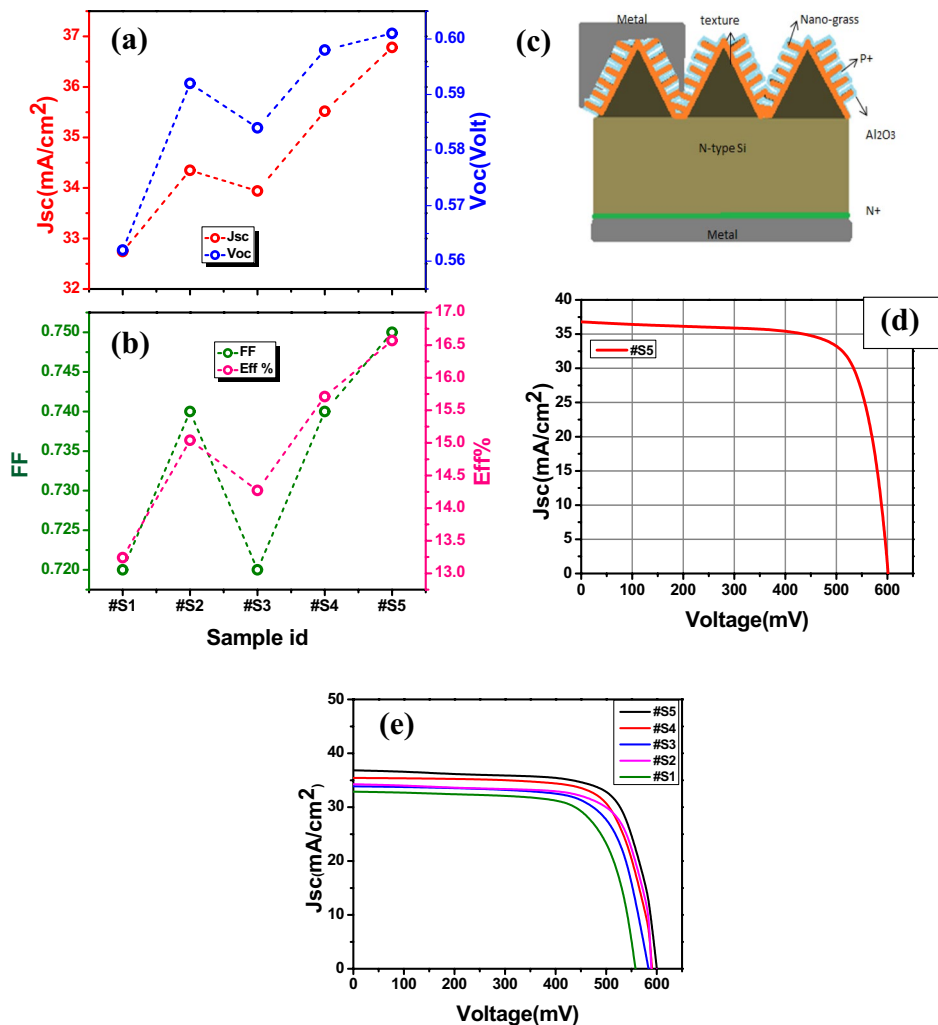


Fig. 6 Lifetime variation with anneal temperature of sol-gel passivation layer

nano-grass was formed in both sides of the wafer leading to enhancement of transmittance followed by reduction of efficiency. This was approved by the result obtained by simulation method. Here front sided nano-grass showed better result than both sided nano-grass structure. Including the idea rear side of the textured wafer was covered by polymer and nano-grass was formed in only front open surface of the wafer. To reduce budget spin on diffusion with RTA technique was carried out on front and rear side of textured nano-grass wafer. Commercial high cost passivation method was replaced here by introducing comparatively low cost and easy technique sol-gel chemical passivation method and finished cell gave better efficiency. More optimization was necessary. This technique could be commercialized in future as low cost high efficiency solar cell.

Fig. 7 Solar cell characterization for different diffusion profile samples, **a** variation of J_{sc} and V_{oc} ; **b** variation of FF and Eff; **c** schematic of complete cell; **d** typical IV of #S5 sample; **e** IV curve of all samples



6 Summary

This work has emphasized a very low cost c-Si Solar cell fabrication. This was a commercially viable technology. The fabrication process was mainly chemical synthesis process. High efficiency solar cell obtained in our first attempt of the work. Modification will lead to betterment of result. The subject of this paper was to fabricate very low cost high efficiency solar cell with commercially viable technology. Silicon nano-grass structure has been formed on textured silicon by chemical etching. During this nanograss was formed on both side of the wafer resulting detrimental effect on optical absorption. So nano-grass was formed only on emitter surface. RTA diffusion has been done with different profile and sheet resistance has been measured accordingly. Al_2O_3 was deposited by sol-gel method. Surface characterization has been done. Lifetime has been measured after annealing. Metallization was done by screen printing. Final structure gave efficiency 16.57%.

Acknowledgement The authors are deeply acknowledged to Mukul K Das and his team for technical and simulation support. The authors are thankful to Prof. Swapan Datta of IEST, Shibpur for giving valuable guidance. The authors are also grateful to the SERI, DST, Govt. of India for financial support for carrying out solar cell related research activity. The authors deeply acknowledge Meghnad Saha Institute of Technology, TIG in providing the infrastructural support for carrying out research activity in this area.

Funding The study has no funding.

Compliance with ethical standards

Conflict of interest The authors declare that they have no conflict of interest.

References

1. Yanto Rahman D, Mamat Rokhmat Elfi Yuliza, Euis Sustini, Mikrajuddin Abdullah (2016) New design of potentially low-cost solar cells using TiO_2 /graphite composite as photon absorber. *Int J Energy Environ Eng* 7:289–296
2. Kumaragurubaran B, Anandhi S (2014) Reduction of reflection losses in solar cell using Anti-Reflective coating. In: International conference on computation of power, energy, information and communication (ICCPIC).
3. Vikas Kumar (2015) Anti-reflection coatings for highly efficient solar cells. National Conference on Photonics and Material Science.
4. Srivastava SK, Kumar D, Singh PK, Kar M, Kumar V, Husain M (2010) Excellent antireflection properties of vertical silicon nanowire arrays. *Solar Energy Mater Solar Cells* 94(9):1506–1511
5. Ramanujam J, Shiri D, Verma A (2011) Silicon nanowire growth and properties: a review. *Mater Express* 1:105–126
6. Li S, Ma W, Yang Zhou, Xiuhua Chen, Yongyin Xiao, Mingyu Ma, Wenjie Zhu, Feng Wei (2014) Fabrication of porous silicon nanowires by MACE method in $\text{HF}/\text{H}_2\text{O}_2/\text{AgNO}_3$ system at room temperature. *Nanoscale Res Lett* 9:196
7. Peng K, Juejun Hu, Yan Y, Yin Wu, Fang H, Ying Xu, Lee ST, Zhu J (2006) Fabrication of single-crystalline silicon nanowires by scratching a silicon surface with catalytic metal particles. *Adv Funct Mater* 16:387–394
8. Rajkumar K, Pandian R, Sankarakumar A, Kumar RTR (2017) Engineering silicon to porous silicon and silicon nanowires by metal-assisted chemical etching: role of Ag size and electron-scavenging rate on morphology control and mechanism. *ACS Omega* 2:4540–4547
9. Martínez J, Moreno M, Rosales P, Torres A, Ambrosio R, Murias D (2016) Study of the spin on dopant technique as alternative for the fabrication of c-Si solar cells. 43rd Photovoltaic specialists conference (PVSC). IEEE, At Portland, OR, USA, pp 2483–2486
10. Soma Ray, Baishakhi Pal, Hemanta Ghosh, Suchismita Mitra, Anup Kumar Mondal, Chandan Banerjee, Hiranmoy Saha, Utpal Gangopadhyay (2020) Effect of induced charges on the performance of different dielectric layers of c-Si solar cell by experimental and theoretical approach. *J Silicon*, vol 23.
11. Makino T (1995) Transfer matrix method with applications to distributed feedback optical devices. *Progress Electromagnetic Res Pier* 10:271–319
12. Nikolai VV, Gorden V, Thomas H (2008) Effective medium theories for irregular fluffy structures: aggregation of small particles. *Optical Soc Am* 46:4065–4072
13. a Bosch Salvador, Ferre-Borrull Josep, Leinfellner Norbert, Canillas Adolf (2000) Effective dielectric function of mixtures of three or more materials: a numerical procedure for computations. *Surface Sci* 453:9–17
14. Mews Mathias, Schultz F. Tim, Mingirulli Nicola, Korte Lars (2013) Hydrogen plasma treatments for passivation of amorphous-crystalline silicon heterojunctions on surface promoting epitaxy. *Appl Phys Lett*, vol 102.
15. Laaksonen K, Li S-Y, Puisto SR, Rostedt NKJ, Ala-Nissil TA, Granqvist CG, Nieminen RM, Niklasson GA (2014) Nanoparticles of TiO_2 and VO_2 in dielectric media: Conditions for low optical scattering, and comparison between effective medium and four-flux theories. *Solar Energy Mater Solar Cells* 130:132–137
16. Yung-Jr H, Lee San-Liang Wu, Kai-Chung TY, Yen-Ting P (2011) Antireflective silicon surface with vertical aligned silicon nanowires realized by simple wet chemical etching processes. *Opt Express* 19:15792–15802
17. Hylton JD, Burgers AR, Sinke WC (1997) Absorption in thin textured silicon wafers, vol 97.
18. Akter Nahid, Mahmood Hasan Zahid, Hoq Mahbulbul, Md. Rafiq Akand Abdur, Basher Mohammad Khairul, Tonima Akter Masuda, Ali Hanif Mohammad (2015) Determination of minority carrier diffusion length by SPV measurement for calculation of carrier generation and recombination of silicon solar cell. In: International conference on materials, electronics & information engineering, ICMEIE, ISBN 978-984-33-8940-4.
19. Ali I, Ramadan MRI, Aboul-Enein S, Abdel-Azeem ElSebaai A, El-Broullesy SM (2011) Short circuit current I as a real non-destructive diagnostic tool of a photovoltaic modules performance. *Int J Renewable Energy Res IJRER* 1(3):53–559
20. Cheknane A, Benouaz T (2009) Prediction model for the diffusion length in silicon-based solar cells. *J Semicond* 30:072001

Publisher's Note Springer Nature remains neutral with regard to jurisdictional claims in published maps and institutional affiliations.